THE METALLIC CHROMOSPHERE AT THE KHARTOUM ECLIPSE

J. B. ZIRKER
Sacramento Peak Observatory, Geophysics Research Directorate, Sunspot, New Mexico
Received October 28, 1957; revised December 23, 1957

ABSTRACT

Logarithmic emission gradients and absolute integrated emission as functions of height are presented for moderately strong metal lines observed at the Khartoum eclipse by the High Altitude Observatory expedition. The gradients are controlled by the combined action of self-absorption and the chromospheric density gradient. Self-absorption is evaluated for a number of metal lines, from which follows an estimate of the density distribution through the low chromosphere The cores of many metallic Fraunhofer lines appear to originate in the chromosphere.

INTRODUCTION

The High Altitude Observatory expedition to the solar eclipse of February 25, 1952, obtained a series of chromospheric spectra distinguished by a combination of great height resolution (100 km) and moderate dispersion (7–11 A/mm). Measurements and analysis of the Balmer lines, the helium lines, and the continuum appearing on the eclipse plates have been published earlier in this *Journal* (Athay *et al.* 1954, 1955; Athay and Thomas 1955; Matsushima, 1955; Athay and Menzel 1956). This paper presents the measurements of a number of moderately strong lines of the metals and of neutral oxygen which appear on the eclipse plates. A preliminary analysis of these data appears in the last section.

For a complete discussion of the observing schedule at the eclipse, the equipment, and the photometric calibration, the reader is referred to the paper of Athay *et al.* (1954). Only the most essential details will be summarized here.

Three grating spectrographs operated throughout the eclipse, providing a dispersion of 7.5 A/mm in the violet (λλ 3360–5100), 11.0 A/mm in the visual (λλ 3950–6500), and 11.5 A/mm in the red. The spectrographs made jumping-film exposures of 0.3-second duration at intervals of 0.4 second in the low chromosphere, corresponding to a 108-km displacement of the moon between consecutive exposures.

Primary and secondary images of the spectrum, differing in intensity by a factor of about 100, are available on each exposure. This feature extends the range of intensities which can be measured accurately and has proved very valuable in the photometric calibration. Originally, Athay estimated the uncertainty of the absolute intensity calibration as ± 0.1 in the logarithm. Athay, Menzel, and Orrall (1956) have recently revised the photometry of the eclipses of 1932 (Cillié and Menzel 1935), 1936 (Hemmendinger 1939), and 1952 (Athay *et al.* 1954). They find that the 1952 intensities (as tabulated here) are too high by a factor of 2. Their correction of -0.3 in the logarithm places the 1952 intensity scale in almost exact agreement with the revised intensities for 1932 but still 0.3 above the 1936 intensities.

REDUCTION OF THE OBSERVATIONS

All metal-line data tabulated here pertain to a point on the east limb at second contact identical with the one Athay *et al.* (1954) discussed (point *b* in their Fig. 1). The point corresponds to a Bailey bead close to the line of contacts at heliographic position angle 65°. This region of the sun showed no prominence activity throughout a period of several

days before and after the eclipse. Coronal-line intensities were also low, so that the region discussed should be characteristic of the quiet chromosphere.

Seventeen spectrograms in the ultraviolet and nineteen in the visible permit accurate microphotometry. The red plates are underexposed, but two interesting triplets (Ca II λλ 8662, 8542, 8498, and O I λλ 7775, 7774, 7772) appear on sixteen plates.

Tracings of the spectrograms were made on the microphotometer at the High Altitude Observatory, specially designed for recording the high photographic densities appearing on the eclipse plates. The tracings cover completely the spectrum from λ 3360 to λ 4500 at fifteen heights and include selected regions from λ 4500 to λ 8700 at twelve heights.

A slit 11 × 120 μ in size was used. This is narrow enough to resolve the grain structure of the films and short enough to remain within the Bailey bead. The slit-width corresponds to 0.083 A on the ultraviolet films, 0.12 A on the visual films, and 0.13 A on the red films. One inch corresponds to 1.1 A on the ultraviolet tracings and 1.6 A on the visible tracings.

The secondary images on the ultraviolet spectrograms were used at heights of 100, 530, 750, and 850 km for $\lambda < 3500$ and at 100 and 530 km for $\lambda > 3500$. Primary images were used at all other heights in the ultraviolet and at all heights on the visual and red spectrograms. During the reduction of the tracings, many strong lines were discovered to be saturated in the primary image on the ultraviolet spectrograms at heights immediately above 530 km. The data at these heights have been included in the least-squares solutions described below but have been given low weight. On the visual plates, no saturation difficulties were encountered. The visual films are, in general, superior in quality to the ultraviolet films.

Menzel's extensive tabulation (1931) of chromospheric lines facilitated the identification of all lines of interest in the wave-length interval covered by the tracings. The reduction was limited to those metallic lines which were free of strong blends according to Menzel's identifications at higher dispersion.

A profile was constructed for each suitable emission line from intensity measurements at intervals of 0.1 A. In slitless spectra the measured profiles of emission lines are usually badly distorted by the effects of seeing and instrumental vibration. Therefore, no attempt was made to recover the true chromospheric profiles from the data. Only the area under each profile was recorded and then converted to absolute units. With few exceptions, a straight line fits each plot of the logarithm of the integrated emission against height, i.e., $E = E_0 \exp - (\beta h)$. Least-squares solutions yielded the slope and intercept of the best straight line through the points

As mentioned above, strong lines at low heights are saturated on the primary images of the ultraviolet films. The areas measured for these heights have large random errors. Consequently, a method was devised to evaluate the weight assigned to each profile in a least-squares solution. The weight of the area under the profile of a line at a given height is defined as the slope of the characteristic curve at the maximum intensity in the line. Thus strongly saturated profiles have central densities lying well up on the knee of the characteristic curve and receive low weight. Very weak lines, lying on the toe of the curve, similarly receive low weight. Only lines whose central densities lie on the linear part of the curve receive the highest weight.

Table 1 lists the integrated emission in each line as a function of height. The emission emanates in all directions from a slice of the chromosphere bounded by two parallel planes 1 cm apart which lie in the line of sight and are perpendicular to the sun's limb and a third plane tangent to the moon's limb along the line of sight. Add 12.00 to the upper number in each entry to obtain the integrated emission. The lower number, where present, represents the weight of the observation in a least-squares solution. Thus for λ 3361, log E at h = 100 km is 12.00 + 3.02 = 15.02, and the weight is 0.77.

An asterisk denotes that the measures were made on the secondary spectrum. All

measures on ultraviolet plates for 100 km and 530 km were made on the secondary image Measurements on visual plates begin with λ 3944.

Table 2 collects the results of least-squares solutions for the natural logarithmic emission gradient (β) and the common logarithm of the integrated emission at $h = 0$ km, log $E(0)$. The errors quoted for the emission gradients are mean (r.m.s.) errors. The upper and lower excitation potentials involved are also given.

The reliability of these data depends upon the errors that may arise in the several steps involved in their determination: (*a*) photography, (*b*) photometric standardization, (*c*) microphotometry of the films, and (*d*) reduction of the tracings. Serious systematic errors probably arise only from the photometric standardization, particularly from the corrections to absolute intensity and from the ratio of intensities in the primary and secondary images. As was mentioned previously, the absolute intensities may all be too large by 0.3 in the logarithm. The ratio of intensities in primary and secondary are probably accurate to within ± 0.1 in the logarithm.

The only way to estimate random errors arising from the microphotometry and reduction of the line profiles is to repeat the entire process. Approximately one hundred profiles appear on two or more tracings and have been used to estimate errors in microphotometry. The maximum difference in the emission of an unsaturated line derived from two tracings is 0.25 in the logarithm, the mean difference is 0.1. Saturated profiles have random errors in the emission as large as 0.5 in the common logarithm.

Athay, Menzel, and Orrall (1956) have compared emission gradients from Table 2 (along with previously published 1952 data for hydrogen and helium) with the corresponding gradients observed at the 1932 and 1936 eclipses. They found no systematic differences among the emission gradients observed at these three eclipses.

Houtgast (1957) has recently published the metallic-line intensities observed by the Utrecht expedition to Khartoum. In order to compare the Utrecht results with those of Table 2, an emission gradient was computed for each line from the difference of the maximum and minimum Utrecht intensities. The r.m.s. difference between the Utrecht gradient and the corresponding HAO gradient was 0.26×10^{-8} for 35 metallic lines. There is a slight tendency for the HAO gradients to be systematically larger: the mean difference among the 35 gradients was $+0.11 \times 10^{-8}$. The HAO intensities, as revised by Athay *et al.* (1956), are larger by about 0.2 in the logarithm than the Utrecht intensities at 530 km. On the whole, the results of the two investigations agree quite well, despite the photometric difficulties inherent in such a comparison and despite the procedure, used by Houtgast, of combining data from several points on the limb.

In contrast, the Pulkovo observations (Vyazanitsyn 1956) of the Khartoum eclipse disagree rather violently with both the HAO and the Utrecht results. A comparison of 19 metallic lines common to the HAO and Pulkovo tabulations reveals an r.m.s. difference of 0.70×10^{-8} among the emission gradients. The Pulkovo gradients are systematically too low: the mean difference is -0.58×10^{-8}. With such large differences among the emission gradients, it is difficult to compare the absolute intensity scales. Near 1300 km, the Pulkovo intensities are about a factor of 2 lower than the revised HAO intensities.

EMISSION GRADIENTS

It is useful at this point to survey the data for any outstanding empirical correlations. Houtgast (1953) has suggested a correlation between the ionization potential of an atom and the emission gradients (β) of its lines, in the sense that β decreases with ionization potential. His correlation rests essentially on four points: H, He, He^+, and the metals, taken as a group Figure 1 shows that no such correlation prevails within the metal group. In this diagram the average value of β for each atom has been plotted against the corresponding ionization potential.

Table 1-A

Integrated Emission

Add 12.00 to convert to ergs/sec/cm

Wavelength (A)	Height (km)																ION
λ	100*	530*	640	750	850	960	1070	1180	1280	1390	1500	1610	1750	1980	2250	2520	
3361	3.02	2.58	1.90	2.42*	2.29*		1.92	1.83	1.81	1.66	1.61	1.68	1.45				Ti^+, Sc^+
	0.77	0.70	0.73	0.72	0.72		0.50	0.63	0.76	0.76	0.76	0.76	0.71				
3368	2.54	2.29	2.06	2.21*	1.99*	1.84	1.84	1.86	1.84	1.71	1.71	1.67	1.41			0.94	Cr^+
	0.77	0.65	0.47	0.72	0.67	0.58	0.76	0.58	0.76	0.76	0.76	0.76	0.76			0.76	
3373	2.98	2.65	2.47	2.55*		2.20	2.16			2.10	2.09	2.04	1.68			1.39	Ti^+
	0.72	0.75	0.05	0.96		0.17	0.23			0.17	0.68	0.30	0.21			0.30	
3380	2.79	2.30	2.07	1.93*	1.75*	1.81	1.73	1.85	1.60	1.49	1.42	1.36	1.11			0.64	Ti^+
	0.77	0.65	0.33	0.72	0.62	0.42	0.70	0.40	0.76	0.83	0.83	0.83	0.83			0.83	
3384	2.92	2.61	2.25	2.49*	2.36*	2.11	2.15	2.18		2.06	1.99	2.02	1.62			1.25	Ti^+
	0.72	0.82	0.15	1.00	0.90	0.08	0.17	0.13		0.23	0.29	0.27	0.26			0.36	
3388	2.97	2.35		2.22	2.16	1.67	1.95	1.80	1.74	1.64	1.60	1.49	1.25			0.81	Ti^+
	0.72	0.69		0.13	0.27	0.43	0.32	0.35	0.45	0.58	0.83	0.83	0.56			0.63	
3394	2.72	2.37	2.09	2.00*	1.99*	1.72	1.88	1.85	1.72	1.52	1.58	1.46	1.31			0.77	Ti^+
	0.75	0.70	0.15	1.00	0.65	0.44	0.30	0.35	0.61	0.70	0.83	0.83	0.58			0.83	
3409	2.54	2.20	1.87	2.05*	2.05*	1.69	1.50	1.60	1.45	1.36	1.23	1.30	0.99			0.68	Cr^+
	0.84	0.70	0.20	0.76	0.68	0.20	0.41	0.34	0.57	0.55	0.91	0.91	0.65			0.72	

1958ApJ...127..680Z

Table 1-A (Continued)

λ	100*	530*	640	750	850	960	1070	1180	1280	1390	1500	1610	1750	1980	2250	2520	
3415	2.28	1.76	1.31	1.15	1.17	1.15	0.96	0.93	0.80	0.64	0.59	0.58	0.00			-.16	Ni
	0.85	0.55	0.48	0.42	0.80	0.91	0.91	0.91	0.91	0.91	0.91	0.91	0.91			0.91	
3421	2.54	1.90	1.81	2.00	1.69	1.70	1.52	1.60	1.50	1.38	1.20	1.14	0.91			0.67	Cr^+
	0.84	0.72	0.23	0.11	0.26	0.27	0.40	0.28	0.62	0.57	0.91	0.91	0.65			0.77	
3422	2.74	2.26	1.82	2.02*	1.85*	1.74	1.56	1.55	1.54	1.48	1.38	1.34	1.09			0.68	Cr^+
	0.84	0.78	0.20	0.82	0.61	0.19	0.38	0.35	0.51	0.47	0.91	0.91	0.50			0.72	
3433	2.72	2.36	1.88	1.94*	1.70*	1.64	1.57	1.68	1.42	1.34	1.28	1.30	1.05			0.63	Cr^+
	0.84	0.80	0.12	0.76	0.54	0.23	0.40	0.26	0.60	0.62	0.91	0.91	0.68			0.91	
3438				1.07	1.11	1.01	0.95	0.71	0.94	1.00	0.37	0.30					Mn^+, Zr^+
				0.49	0.60	0.91	0.91	0.91	0.91	0.91	0.91	0.91					
3442	2.59	2.15	2.01	2.12*	1.99*	1.70		1.69	1.61	1.53	1.61	1.45	1.20			0.87	Mn^+
	0.84	0.79	0.15	1.09	0.70	0.24		0.20	0.30	0.32	0.41	0.58	0.33			0.42	
3444	2.61	2.12	1.76	1.88*	1.84*	1.59	1.49	1.31	1.38	1.15	1.05		0.74			0.29	Ti^+
	0.85	0.70	0.23	0.70	0.50	0.30	0.40	0.45	0.47	0.91	0.91		0.91			0.91	
3446	2.36	1.57	1.25	1.05	1.11	1.05	0.84	0.74	0.66	0.51	0.52	0.26	0.17				Ni^+
	0.86	0.55	0.47	0.49	0.64	0.87	0.35	0.91	0.91	0.91	0.91	0.91	0.91				
3456	2.51	1.73	1.13	1.72	1.74	1.03	1.02	0.99	0.87	0.63	0.47	0.33	0.25				Ti^+
	0.85	0.57	0.45	0.35	0.64	0.83	0.91	0.91	0.91	0.91	0.91	0.91	0.91				
3460	2.68	2.18	1.99	1.90*	1.75*	1.85	1.67	1.58	1.56	1.38	1.36	1.14	1.03			0.59	Mn^+
	0.82	0.84	0.12	0.94	0.55	0.16	0.20	0.23	0.30	0.43	0.64	0.91	0.50			0.66	
3461	2.64	2.15	1.76	1.86	1.75	1.59	1.53	1.38	1.36	1.13	1.10	0.89	0.70			0.43	Mn^+, Ti^+
	0.84	0.77	0.20	0.70	0.32	0.30	0.38	0.47	0.63	0.84	0.91	0.91	0.91			0.91	

Table 1-A (Continued)

λ	100*	530*	640	750	850	960	1070	1180	1280	1390	1500	1610	1750	1980	2250	2520	
3474	2.54	2.30	1.94	2.08*	2.01*	1.77	1.69	1.54	1.60	1.34	1.39	1.25	1.16			0.74	Mn^+
	0.83	0.85	0.15	0.80	0.60	0.20	0.15	0.33	0.30	0.47	0.84	0.91	0.41			0.45	
3475	2.64	2.08	1.59	1.47	1.62	1.04	0.90	0.87	0.71	0.77	0.77	0.61	0.30				Fe
	1.20	0.62	0.37	0.40	0.58	0.84	1.05	1.15	0.85	0.98	0.86	0.83	0.97				
3477	2.67	2.37	1.93	2.19*	2.08*	1.50	1.10	1.28	1.05	1.16	1.10	0.90	0.71				Ti^+
	0.96	0.86	0.26	0.86	0.61	0.50	0.74	0.58	1.10	1.05	1.04	0.93	0.91				
3479	2.80		1.21		1.19	0.76											Zr^+
	1.16		1.00		1.20	0.96											
3481	2.43	1.76	1.08		1.23	0.86	0.91	0.43									Zr^+
	1.24	0.54	0.84		1.10	1.02	0.87	0.88									
3483	2.74	2.21	1.85	1.74	1.67	1.33	1.26	1.36	1.11	1.12	1.15	1.10	0.83				Mn^+
	1.16	0.79	0.25	0.30	0.34	0.68	0.81	0.54	1.10	0.66	1.10	1.05	0.77				
3489	2.76	2.15	1.82	2.30*	1.80*	1.34	1.32	1.32	1.20	1.27	1.19	1.24	0.98				Mn^+
	1.08	0.77	0.27	0.70	0.50	0.59	0.84	0.68	1.15	1.71	1.05	1.15	0.48				
3491	2.41	2.38	1.79	2.18*	2.00*	1.46	1.40	1.28	1.21	1.25	1.12	1.05	0.77				Fe, Ti^+
	1.05	0.82	0.28	0.73	0.55	0.64	0.86	0.71	1.15	0.94	1.04	1.00	0.98				
3493	2.65	2.08	1.69	1.63	1.27	1.12	1.07	1.06	0.75	1.01	0.81	0.83	0.49				Ni
	1.19	0.61	0.38	0.42	0.60	0.86	1.15	0.98	0.84	0.96	0.86	0.84	1.05				
3505	2.91	2.34	2.13	2.18*	1.88	1.43	1.35	1.32	1.25	1.21	1.18	1.12	0.85				Ti^+
	0.99	0.86	0.15	0.87	0.21	0.54	0.64	0.59	0.84	0.66	1.10	1.04	0.54				
3511	2.90	2.37	2.15	1.71*	1.68*	1.46	1.28	1.34	1.15		1.09	0.93	0.79				Ti^+
	0.91	0.86	0.18	0.71	0.49	0.50	0.73	0.59	1.05		1.05	1.06	0.63				

1958ApJ...127..680Z

Table 1-A (Continued)

λ	100*	530*	640	750	850	960	1070	1180	1280	1390	1500	1610	1750	1980	2250	2520	
3515	2.62	1.96		1.50	1.36	1.14	0.97	0.95	0.79	0.66		0.40	0.35				Ni
	1.15	0.64		0.15	0.58	0.84	1.12	0.98	0.96	1.00		0.84	1.05				
3520	2.74	2.03	1.58	1.52	1.30	1.11	0.92	1.01	0.72	0.76	0.82						Ti^+
	1.03	0.64	0.43	0.28	0.65	0.74	1.12	0.88	0.87	0.88	0.93						
3524	2.91	2.07	1.61	1.48	1.66	1.22	0.96	1.06	0.86	0.84	0.80	0.70	0.59				Ni
	1.01	0.66	0.41	0.40	0.34	0.60	0.91	0.71	0.93	1.10	0.88	0.86	1.02				
3535	2.87	2.33	1.94	1.93*	1.67*	1.35	1.29	1.23	1.00	1.07	1.07	0.90	0.84				Ti^+
	0.79	0.82	0.30	0.70	0.43	0.54	0.84	0.88	1.04	1.06	0.99	0.96	0.95				
3545	2.64	1.96	1.47	1.20	1.36	1.01	0.90	0.78	0.56	0.62	0.75	0.58					V^+
	1.12	0.63	0.42	0.49	0.45	0.83	1.12	1.15	0.88	0.93	0.88	0.86					
3556	2.75	2.25	1.61	1.81	1.27	1.22	0.97	1.06	0.80	0.73	0.74	0.57	0.41				V^+
	0.89	0.75	0.40	0.28	0.77	0.70	0.88	0.84	1.03	1.04	0.88	0.88	0.98				
3558	2.64	2.16	1.61	1.50	1.71	1.20	1.01	1.12	0.77	0.93	0.77	0.61					Sc^+
	1.05	0.72	0.37	0.38	0.35	0.60	0.92	0.68	0.93	1.10	0.89	0.90					
3568		2.05	1.55	1.74	1.53	1.14	1.05	1.26	0.90	0.69	0.86						Sc^+
		0.68	0.39	0.25	0.35	0.70	0.92	0.92	0.93	1.06	0.90						
3570	2.62	2.14	1.77	1.65*		1.39	1.27		1.16	0.92	0.99	0.85	0.71				Fe
	1.19	0.78	0.14	0.67		0.30	0.45		0.70	0.75	1.20	1.22	0.70				
3576	2.69	2.30	1.54	2.14*	1.88*	1.48			1.27	0.91	1.00	0.81	0.64				Sc^+
	1.03	0.87	0.24	0.76	0.42	0.30			0.68	0.90	1.05	1.15	0.92				
3579		2.04		1.70*	1.61*	1.15	1.12		1.13	0.74	0.85	0.77	0.40				Cr^+
		0.72		0.56	0.44	0.38	0.60		0.70	1.05	1.15	1.15	1.00				

1958ApJ...127..680Z

Table 1-A (Continued)

λ	100*	530*	640	750	850	960	1070	1180	1280	1390	1500	1610	1750	1980	2250	2520	
3581	2.68	2.31	1.66	2.18*	1.94*	1.59	1.46		1.36	1.18	1.04	1.02	0.86				Fe
	1.10	0.89	0.21	0.56	0.51	0.20	0.35		0.53	0.41	0.75	1.15	0.55				
3596	2.13	1.91	1.49			1.15	0.87		0.81	0.83	0.80	0.41	0.41				Ti^+
	1.17	0.67	0.32			0.50	0.85		1.15	1.17	1.13	1.05	1.07				
3609		1.94	1.55	1.39	1.39	1.05	1.16		1.06	0.81	0.82	0.63	0.60				Fe
		0.69	0.26	0.27	0.29	0.45	0.50		0.90	1.10	1.19	1.17	1.00				
3614	2.57	1.29			1.54	1.62	1.41		1.40	1.24	1.10	1.02	0.94				Sc^+
	0.96	0.98			0.25	0.11	0.27		0.34	0.56	0.83	0.97	0.43				
3625	2.52	2.03	1.62	1.40	1.31	1.42	1.05		1.08	0.67	0.79	0.68	0.51				Ti^+
	1.00	0.77	0.30	0.25	0.45	0.17	0.60		0.70	1.10	1.15	1.12	0.73				
3641	2.61	2.18	1.59	1.62	1.43	1.43	1.28		1.12	0.94	0.94	0.78	0.53				Ti^+
	1.02	0.87	0.18	0.30	0.34	0.25	0.28		0.78	0.70	1.15	1.15	0.77				
3643	2.65	2.29	1.57	1.56	1.66	1.81	1.33		1.20	0.88	1.10	0.72	0.67				Sc^+
	1.00	0.93	0.18	0.27	0.11	0.12	0.41		0.55	0.87	0.93	1.17	0.67				
3645	2.56	2.01	1.70	1.56		0.98	0.90		0.99	0.74	0.71						Sc^+
	1.09	0.74	0.24	0.27		0.40	0.70		0.87	1.20	1.13						
3648	2.58	2.11	1.40	1.69	1.32	1.35	1.17		1.15			0.74	0.55				Fe
	1.12	0.75	0.45	0.23	0.25	0.32	0.60		1.15			1.20	0.87				
3685	2.92	2.91	1.87	1.83	2.30	1.95	2.19		2.34	2.07		2.01	1.49				Ti^+
	0.69	0.58	0.16	0.18	0.02	0.15	0.07		0.00	0.07		0.07	0.14				
3709			2.24	0.98	0.88	0.91	0.60	0.64	0.49	0.47							Fe
			0.08	0.38	0.57	0.66	1.05	1.00	0.77	1.17							

1958ApJ...127..680Z

Table 1-A (Continued)

λ	100*	530*	640	750	850	960	1070	1180	1280	1390	1500	1610	1750	1980	2250	2520	
3710	2.64	2.14	2.69	1.42	1.32	1.16	1.00	0.94	0.83	0.54	0.46	0.32					Y^+
	1.07	0.80	0.17	0.21	0.35	0.33	0.62	0.70	0.79	0.93	1.05	1.05					
3720	2.57	2.30	2.74	1.64	1.68	1.68	1.58	1.67	1.83	1.34	1.21	1.15					Fe
	0.66	1.10	0.20	0.17	0.16	0.10	0.15	0.05	0.15	0.27	0.53	0.47					
3742	2.74	2.21	2.69	1.28	1.60	1.44	1.22	1.20	1.46	0.88	0.81	0.77	0.64				Ti^+
	1.05	1.00	0.20	0.35	0.23	0.15	0.33	0.36	0.51	0.73	0.97	1.03	0.45				
3746	2.86	2.28	2.82	1.67	1.77	1.58	1.45	1.51	1.47	1.19	1.05	1.05	0.75				Fe
	1.10	1.05	0.20	0.17	0.16	0.16	0.11	0.19	0.25	0.47	0.81	0.48	0.55				
3748	2.72	2.12	2.75	1.52		1.23	1.33	1.36	1.22	1.21	0.68	0.86					Ti^+, Fe
	1.12	0.77	0.20	0.19		0.37	0.20	0.19	0.42	0.66	1.02	0.94					
3759	3.16	2.91					1.96	1.22	2.09	1.56	1.98	1.87	1.42				Ti^+
	0.72	0.50					0.05	0.02	0.03	0.35	0.17	1.17	0.21				
3761	3.14	2.84	3.09	1.97	2.00	1.76	1.97	1.90	1.86	1.70	1.09	1.83					Ti^+
	0.73	0.63	0.13	0.12	0.58	0.12	0.03	0.05	0.19	0.20	0.14	0.21					
3764	2.79	2.02	1.45	1.54	1.42	1.19	1.04	1.08	0.93	0.91	0.72	0.71					Fe
	1.18	0.60	0.50	0.19	0.47	0.45	0.57	0.57	0.87	0.73	1.08	1.09					
3767	2.73	1.87	1.56	1.12	1.18	1.07	0.81	0.78	0.81		0.60	0.64					Fe
	1.20	0.56	0.27	0.38	0.50	0.53	0.87	0.83	0.81		1.17	1.15					
3774	2.64	2.14	2.62	1.12	1.14	0.99	0.78	0.81	0.85	0.54	0.54	0.49					Y^+
	1.05	0.82	0.16	0.41	0.47	0.64	0.87	0.73	1.03	1.03	1.05	1.17					
3789	2.84	1.90	1.40	0.99	0.97	0.86	0.60		0.38								Y^+
	1.05	0.57	0.27	0.47	0.59	0.57	1.20		1.20								

1958ApJ...127..680Z

Table 1-A (Continued)

λ	100*	530*	640	750	850	960	1070	1180	1280	1390	1500	1610	1750	1980	2250	2520	
3795			2.37	1.05		0.88											Fe
			0.21	0.67		0.77											
3799			2.46	1.28	1.06	1.12	0.95	0.90	0.85			0.71					Fe
			0.27	0.32	0.71	0.62	1.07	0.90	1.23			1.12					
3813	2.92		2.54	0.82	0.93	0.93	0.70	0.63		0.54	0.63						Ti^+
	1.09		0.24	0.70	0.71	0.80	1.17	1.05		1.10	1.05						
3814	2.91		2.37		0.94	0.84	0.63	0.55	0.53	0.47	0.33						Ti^+
	1.12		0.30		0.73	0.75	1.13	0.98	1.15	1.07	1.05						
3816	2.90	2.07	2.61	1.27	1.36	1.32	1.03	0.98	1.04	0.73	0.78	0.74					Fe
	1.12	0.71	0.20	0.27	0.37	0.19	0.16	0.65	0.80	0.80	1.05	1.09					
3820			2.82	1.45	1.63	1.32	1.28	1.41	0.98	0.99	1.08		0.41				Fe
			0.12	0.27	0.27	0.18	0.33	0.19	0.33	0.63	0.75		0.66				
3824		2.02	1.59	1.31	1.42	1.32	1.09	1.10	0.98	0.58	0.80	0.70					Fe
		0.76	0.20	0.20	0.31	0.33	0.55	0.45	0.73	0.94	1.05	1.03					
3826		2.09	2.60	1.23	1.51	1.39	1.07	1.20	1.15	0.87	0.74	0.96	0.41				Fe
		0.82	0.19	0.31	0.24	0.25	0.43	0.33	0.57	0.64	1.05	0.77	0.61				
3827	2.90	1.95	2.86	0.97	1.29	1.25	0.87	0.73	0.77	0.57	0.31	0.65	0.50				Fe
	1.10	0.61	0.19	0.53	0.33	0.33	0.80	0.83	0.91	0.86	1.15	1.07	0.71				
3829	2.09	2.20	1.77	1.84		1.62		1.48	1.98		1.24	1.35	1.25				Mg
	1.23	1.20	0.15	0.16		0.23		0.23	0.14		0.34	0.31	0.19				
3832	2.60	2.51	1.95	1.94	2.12	1.85	1.77	1.36			1.82	1.76	1.67				Mg
	1.23	1.33	0.15	0.17	0.14	0.11	0.17	0.23			0.17	0.17	0.13				

1958ApJ...127..680Z

Table 1-A (Continued)

λ	100*	530*	640	750	850	960	1070	1180	1280	1390	1500	1610	1750	1980	2250	2520	
3838	2.56	2.50	1.95	1.99	2.20	1.98	1.78	1.74	1.98		1.91	1.87	1.63				Mg
	1.23	1.00	0.16	0.16	0.13	0.15	0.18	0.49	0.13		0.18	0.17	0.13				
3850		1.62	0.86	1.32	0.94	0.63	0.52										Fe
		0.47	0.68	0.30	0.40	1.02	1.02										
3856		2.09	1.45	1.79	1.62	1.46	1.19	1.29	1.22		0.66	0.92	0.73				Fe
		0.92	0.25	0.14	0.48	0.24	0.31	0.28	0.38		1.02	0.74	0.40				
3860		2.29	1.60	1.83	2.13	1.69	1.47	1.74	1.85		1.27	1.41	1.13				Fe
		1.40	0.25	0.16	0.10	0.16	0.25	0.18	0.19		0.33	0.22	0.20				
3865		1.54	0.77	1.31	0.96	0.62	0.41	0.40	0.15								Fe
		0.40	0.70	0.27	0.35	0.65	1.02	0.92	1.02								
3879	2.25	2.16	1.59	1.80	1.67	1.37	1.19	1.18	0.95		0.58	0.99	0.65				Fe
	1.23	0.92	0.17	0.18	0.21	0.27	0.35	0.37	0.51		1.02	0.74	0.40				
3886	2.49	2.24				1.62	1.49		1.44			1.35					Fe
	1.23	1.15				0.24	0.28		0.49			0.39					
3944		1.68	1.48	1.41	1.36	1.12	1.12	1.06	0.76	0.82	0.58	0.24	0.38				Al
3962		1.73	1.72	1.73	1.63	1.39	1.48	1.36	1.16	1.10	1.10	0.71	0.74				Al
3983		1.40	1.18	0.98	0.76												Y^+
4005		1.37	1.20	1.03	0.84	0.52	0.59	0.47	0.12								Fe
4031		1.67	1.56	1.36	1.28	1.03	1.07	0.97	0.56	0.46	0.37	0.23					Mn

Table 1-A (Continued)

λ	100*	530*	640	750	850	960	1070	1180	1280	1390	1500	1610	1750	1980	2250	2520	
4033		1.56	1.41	1.36	1.14	0.81	0.93	0.67		0.44	0.41						Mn
4034		1.52	1.45	1.30	1.02	0.82	0.78	0.73	0.39	0.25	0.26						Mn
4046		1.84	1.79	1.70	1.57	1.29	1.28	1.22	0.95	0.85	0.88	0.69	0.51				Fe
4064		1.73	1.62	1.43	1.37	1.07	1.09	0.95	0.73	0.66	0.57	0.41	0.23				Fe
4072		1.70	1.60	1.44	1.31	1.11	1.04	0.87	0.65	1.53	0.44	0.31	0.26				Fe
4078		2.39	2.35	2.32	2.26	2.10	2.15	2.03	1.96	2.00	1.92	1.76	1.67	1.51	1.29		Sr^+
4144		1.65	1.42	1.19	1.09	0.98	0.97	0.73									Fe
4164		1.55	1.32	0.95	0.97	0.77	0.70										Ti^+
4199		1.37	1.26	0.99	0.87	0.78	0.58										Fe
4202		1.42	1.21	1.00	0.94	0.66	0.62										Fe
4215		2.24	2.30	2.22	2.21	2.15	1.95	1.89	1.72	1.78	1.65	1.61	1.43				Sr^+
4227		1.98	2.12	1.93	1.87	1.76	1.66	1.57	1.46	1.43	1.20	1.10	0.91				Ca
4233		1.86	1.79	1.52	1.41	1.29	0.98	1.00	0.78	0.66	0.69	0.50	0.37				Fe^+
4236		1.31	1.15	0.71	0.70		0.24										Fe
4247		2.06	2.02	1.93	1.87	1.74	1,52	1.47	1.39	1.28	1.09	1.00	0.77				Sc^+

1958ApJ...127..680Z

Table 1-A (Continued)

λ	100*	530*	640	750	850	960	1070	1180	1280	1390	1500	1610	1750	1980	2250	2520	
4251		1.55	1.35	1.02	1.00	0.69	0.51	0.31									Fe
4254		1.77	1.81	1.62	1.58	1.44	1.19	1.10	0.91	0.92	0.79	0.64	0.38				Cr
4260		1.59	1.41	1.10	1.00	0.84	0.66										Fe
4272		1.73	1.65	1.33	1.09	1.03	0.87	0.81	0.70	0.71	0.50	0.27					Fe
4275		1.80	1.80	1.54	1.52	1.36	1.08	0.99	0.87	0.72	0.64	0.48	0.35				Cr
4290		2.07	2.02	1.75	1.69	1.46	1.31	1.18	1.00	1.05	0.89	0.59	0.50				Cr, Ti^+
4294		1.77	1.78	1.60	1.49	1.26	1.19	1.03	0.90	0.87	0.78	0.64	0.47				Ti^+
4300		2.05	1.93	1.73	1.65	1.43	1.28	1.19	1.12	1.07	1.00	0.71	0.57				Ti^+
4321		1.75	1.76	1.43	1.30	1.10	0.91	0.80	0.77	0.49	0.54	0.48					Ti^+, Sc^+
4325		1.94	1.85	1.64	1.55	1.36	1.17	1.11	0.99	0.91	0.83	0.69	0.44				Fe, Sc^+
4383		1.84	1.83	1.69	1.66	1.43	1.31	1.25	1.12	0.92	0.78	0.61	0.72				Fe
4395		2.05	2.05	1.88	1.86	1.60	1.57	1.54	1.29	1.26	1.18	0.94	0.90				Ti^+
4405		1.66	1.56	1.30	1.24	1.05	0.96	0.88	0.73	0.59							Fe
4444		1.97	1.96	1.87	1.77	1.62	1.47	1.43	1.21	1.16	1.04	0.91	1.02				Ti^+
4450		1.59	1.36	0.98	0.99	0.83	0.90	0.90	0.63	0.34	0.14						Ti^+

Table 1-A (Continued)

λ	100*	530*	640	750	850	960	1070	1180	1280	1390	1500	1610	1750	1980	2250	2520	
4468		2.00	1.91	1.80	1.74	1.53	1.49	1.35	1.29	1.15	1.10	0.84	0.97				Ti^+
4501		1.95	1.90	1.71	1.68	1.44	1.39	1.32	1.16	1.02	1.02		0.57				Ti^+
4508		1.32	1.16	0.62	0.62	0.65											Fe^+
4515		1.32	1.06	0.78	0.80	0.65											Fe^+
4520		1.34	0.99	0.75	0.64	0.68											Fe^+
4534		2.07	1.95	1.79	1.73	1.58	1.45	1.41	1.23	1.06	0.95	0.83	0.54				Ti^+, Fe^+
4549		2.13	1.95	1.85	1.87	1.57	1.47	1.42	1.29	1.12	1.06	0.96	0.63				Ti^+
4554		2.14	1.98	1.93	1.88	1.66	1.58	1.52	1.31	1.16	1.05	0.82	0.50				Ba^+
4559		1.37	1.33	1.04	0.97	0.83	0.79	0.64	0.62			0.19					Cr^+
4564		1.94	1.82	1.60	1.60	1.37	1.26	1.22	1.13	0.96	0.85	0.68					Ti^+
4572		2.02	1.89	1.74	1.74	1.55	1.41	1.33	1.20	1.12	0.99	0.86	0.60				Ti^+
4584		1.84	1.72	1.48	1.45	1.15	1.01	0.95	0.87		0.49	0.30					Fe^+
5167			2.11	2.01	2.02	1.70	1.70	1.57	1.38	1.33	1.15	0.96	0.87	0.74	0.36		Mg
5169			2.17	2.03	1.98	1.79	1.67	1.59	1.39	1.26	1.10	0.84	0.69	0.53	0.16		Fe^+
5173			2.34	2.20	2.23	2.18	2.00	2.04	1.86	1.76	1.63	1.47	1.40	1.17	0.93		Mg

1958ApJ...127..680Z

Table 1-A (Continued)

λ	100*	530*	640	750	850	960	1070	1180	1280	1390	1500	1610	1750	1980	2250	2520	
5184			2.44	2.26	2.28	2.39	2.12	2.21	2.06	1.99	1.85	1.70	1.66	1.44	1.17		Mg
5189			1.23	1.18	1.08		0.94	0.86	0.60	0.72							Ti^+
5198			0.99	0.85	0.71		0.51	0.60	0.30								Fe^+
5205			1.27	1.13	1.04	0.81	0.76	0.74									Cr
5206			1.51	1.37	1.26	1.05	0.90	0.90	0.68	0.49							Cr
5208			1.56	1.39	1.30	1.11	0.90	0.96	0.69	0.66							Cr
5233			0.75	0.72	0.65	0.50	0.35	0.46									Fe
5235			1.07	0.92	0.85	0.62	0.62	0.57									Fe^+
5890		2.12		2.05	1.95	1.91	1.84	1.81	1.65	1.64	1.45	1.30	1.19	1.01	0.50	0.45	Na
5895		2.15	2.14	2.06	1.90	1.85	1.64	1.71	1.51	1.45	1.21	1.15	1.03	0.81	0.54		Na

1958ApJ...127..680Z

Table 1-B

λ	100	530	640	750	850	960	1070	1180	1280	1390	1500	1610	1750	1980	2250	2520	3060	3870	4680	5490	6300	
7772	2.99		2.52	2.56		2.23		2.12	1.98	1.83	1.82	1.71		1.55	1.59		0.91	0.30				O
7774	2.94		2.34	2.41		2.10		1.99		1.76				1.46	1.44		0.67					O
7775	2.73	2.23	2.30	2.24		1.94		1.83						1.53		1.13						O
8498	3.37	2.22				2.56		2.36	2.45	2.25	1.99	1.96		1.90	1.80	1.71	1.02	0.45	-.03			Ca^+
8542	3.50	2.21								2.73	2.75	2.52		2.38	2.40	2.23		1.29	0.80		-.06	Ca^+
8662	3.07	2.80	2.73	2.77		2.50		2.45	2.51	2.49	2.31	2.31		2.09	2.16	1.76	1.46	0.84	0.36			Ca^+
3968			4.12				4.01				3.81		3.81				3.39	3.21		2.66		Ca^+

1958ApJ...127..680Z

Table 2

Logarithmic Emission Gradients and Absolute Integrated Emission at Base of Chromosphere

Element	Multiplet	J	λ (A)	β ($\times 10^8$)	Log E(0)	E.P. (Volts)	
O	$3^5S^o - 3^5P$	2-3	7772.0	1.57 ± .07	14.93	9.11	10.69
		2-2	7774.2	1.64 ± .10	14.88	9.11	10.69
		2-2	7775.4	1.44 ± .12	14.68	9.11	10.69
Na	$3^2S - 3^2P^o$	1/2 - 3/2	5890.0	2.12 ± .11	14.78	0.00	2.10
		1/2 - 1/2	5895.9	2.26 ± .07	14.75	0.00	2.09
Mg	$3^3P^o - 3^3D$	0-1	3829.4	1.71 ± .19	14.48	2.70	5.92
		1-2	3832.3	1.93 ± .30	14.84	2.70	5.92
		2-3	3838.3	1.74 ± .22	14.81	2.70	5.92
	$3^3P^o - 4^3S$	0-1	5167.3	2.55 ± .09	14.85	2.70	5.09
		1-1	5172.7	2.21 ± .07	15.09	2.70	5.09
		2-1	5183.6	2.16 ± .03	15.28	2.70	5.09
Al	$3^2P^o - 4^2S$	3/2 - 1/2	3944.0	2.57 ± .17	14.27	0.01	3.13
		1/2 - 1/2	3961.5	2.05 ± .15	14.34	0.00	3.13
Ca	$4^1S - 4^1P^o$	0-1	4226.7	2.16 ± .13	14.63	0.00	2.92
Ca^+	$4^2S - 4^2P^o$	1/2 - 1/2	3968.5	0.68 ± .02	16.31	0.00	3.11
	$3^2D - 4^2P^o$	3/2 - 3/2	8498.1	1.65 ± .07	15.38	1.69	3.14
		5/2 - 3/2	8542.1	1.33 ± .04	15.57	1.69	3.14
		3/2 - 1/2	8662.1	1.33 ± .05	15.19	1.69	3.11

1958ApJ...127..680Z

Table 2 (Continued)

Element	Multiplet	J	λ (A)	β (x 10^8)	log E(0)	E. P. (Volts)	
Sc^+	$a^3D - Z^3D^o$	2-3	3558.5	3.06 ± .20	14.49	0.01	3.48
		1-2	3567.7	2.86 ± .34	14.52	0.00	3.46
		2-2	3576.3	2.95 ± .19	14.85	0.01	3.46
	$a^3D - Z^3F^o$	3-4	3613.8	2.43 ± .13	14.70	0.02	3.44
		1-2	3642.8	2.83 ± .19	14.75	0.00	3.39
		3-3	3645.3	3.29 ± .26	14.71	0.02	3.41
	$a^1D_2 - Z^1D_2$	2-2	4246.8	2.46 ± .09	14.71	0.31	3.22
Ti^+	$a^4F - Z^4G^o$	7/2 - 9/2	3361.2	1.93 ± .27	14.86	0.03	3.70
		5/2 - 7/2	3372.8	1.48 ± .11	14.95	0.01	3.67
		9/2 - 9/2	3380.3	1.92 ± .11	14.65	0.05	3.70
		3/2 - 5/2	3383.7	1.57 ± .08	14.95	0.00	3.55
		5/2 - 5/2	3394.6	1.79 ± .08	14.68	0.01	3.65
	$b^4F - Z^4G^o$	9/2 - 11/2	3444.3	2.26 ± .10	14.58	0.15	3.73
		7/2 - 9/2	3461.5	2.24 ± .14	14.57	0.13	3.70
		5/2 - 7/2	3477.0	2.56 ± .15	14.75	0.12	3.67
		3/2 - 5/2	3491.1	2.44 ± .22	14.67	0.11	3.65
	$b^2P - Y^2P^o$	3/2 - 3/2	3456.4	2.91 ± .23	14.37	2.05	5.62
	$b^2G - Y^2G^o$	9/2 - 9/2	3504.9	2.83 ± .21	14.92	1.88	5.40
		7/2 - 7/2	3510.8	2.93 ± .20	14.87	1.88	5.40
	$a^2F - Z^4D^o$	7/2 - 5/2	3596.1	2.58 ± .19	14.31	0.60	4.04
	$a^2P - ZS^o$	3/2 - 1/2	3641.3	2.79 ± .14	14.69	1.23	4.62

1958ApJ...127..680Z

Table 2 (Continued)

Element	Multiplet	J	λ (A)	β_8 ($\times 10^8$)	log E(0)	E.P. (Volts)	
	$a^2F - Z^2D^o$	7/2 - 5/2 5/2 - 3/2	3685	1.85	15.2	0.60	3.95
	$b^2D - Y^2D^o$	5/2 - 5/2	3741.6	3.05 ± .26	14.84	1.57	4.87
	$a^2F - Z^2F^o$	7/2 - 7/2	3756.3	2.18 ± .23	15.26	0.60	3.89
		5/2 - 5/2	3761.4	2.31 ± .40	15.16	0.57	3.85
	$a^2G - Z^2G^o$	9/2 - 9/2	3900.0	1.94 ± .29	14.46	1.13	4.29
		7/2 - 7/2	3913.5	2.25 ± .29	14.58	1.13	4.26
	$a^2D - Z^2D^o$	5/2 - 5/2	4294.1	2.55 ± .10	14.39	1.08	3.95
	$a^4D - Z^4D^o$	5/2 - 7/2	4300.1	2.68 ± .12	14.61	1.18	4.05
	$a^2D - Z^2F^o$	5/2 - 7/2	4395.0	2.35 ± .11	14.65	1.08	3.89
		3/2 - 5/2	4443.8	2.39 ± .07	14.59	1.08	3.85
		5/2 - 5/2	4450.5	2.86 ± .36	14.12	1.08	3.85
	$a^2G - Z^2F$	9/2 - 7/2	4468.5	2.23 ± .10	14.51	1.13	3.89
		7/2 - 5/2	4501.3	2.52 ± .11	14.55	1.11	3.85
	$a^2H - Z^2G^o$	11/2 - 9/2	4549.5	2.63 ± .11	14.71	1.58	4.29
		9/2 - 7/2	4572.0	2.54 ± .07	14.60	1.56	4.26
	$a^2P - Z^2D^o$	1/2 - 3/2	4563.8	2.57 ± .11	14.50	1.22	3.92
	$b^2D - Z^2D^o$	5/2 - 5/2	5188.7	1.83 ± .19	13.77	1.57	3.95

1958ApJ...127..680Z

Table 2 (Continued)

Element	Multiplet	J	λ (A)	β ($\times 10^8$)	log E(0)	E. P. (Volts)	
Cr	$a^7S - Y^7P^o$	3-4	3578.7	2.61 ± .22	14.47	0.00	3.45
	$a^7S - Z^7P^o$	3-4	4254.3	2.70 ± .12	14.49	0.00	2.90
		3-3	4274.8	2.93 ± .10	14.52	0.00	2.89
	$a^5S - Z^5P^o$	2-1	5204.5	2.43 ± .32	13.93	0.94	3.31
		2-2	5206.0	3.02 ± .17	14.36	0.94	3.31
		2-3	5208.4	2.79 ± .16	14.33	0.94	3.31
Cr^+	$a^4D - Z^6D^o$	7/2 - 5/2	3368.1	1.41 ± .09	14.53	2.47	6.14
	$a^4D - Z^4P^o$	7/2 - 5/2	3408.8	1.90 ± .11	14.57	2.47	6.09
		1/2 - 1/2	3421.3	1.82 ± .12	14.47	2.41	6.02
		3/2 - 3/2	3422.7	1.81 ± .09	14.56	2.44	6.05
		3/2 - 1/2	3433.3	2.00 ± .12	14.63	2.42	6.02
	$a^4P - Z^4P^o$	5/2 - 3/2	3677.7	2.76 ± .21	14.42	2.69	6.05
	$b^4F - Z^4D^o$	9/2 - 7/2	4558.7	2.46 ± .15	13.91	4.06	6.76
Mn	$a^6S - Z^6P^o$	5/2 - 7/2	4030.8	3.15 ± .11	14.45	0.00	3.06
		5/2 - 5/2	4033.1	2.90 ± .14	14.25	0.00	3.06
		5/2 - 3/2	4034.5	3.29 ± .20	14.33	0.00	3.06
Mn^+	$a^5D - Z^5P^o$	4-3	3442.0	1.66 ± .11	14.60	1.77	5.35
		3-2	3460.3	2.00 ± .08	14.64	1.80	5.37
		2-1					
		3-3	3474.1	2.04 ± .10	14.70	1.80	5.35
		2-2	3483.0	2.87 ± .29	14.88	1.82	5.37
		1-1	3488.7	2.77 ± .33	14.89	1.84	5.38

1958ApJ...127..680Z

Table 2 (Continued)

Element	Multiplet	J	(A)	β (x 10^8)	log E(0)	E.P. (Volts)	
Fe	$a^5F - Z^3G^o$	4-5	3570.0	2.66 ± .11	14.66	0.91	4.37
	$a^5F - Z^5G^o$	5-6	3581.2	2.68 ± .25	14.78	0.86	4.30
		1-2	3608.0	2.29 ± .20	14.26	1.01	4.43
		4-5	3647.9	2.72 ± .22	14.58	0.91	4.29
	$a^5D - Z^5F^o$	2-1	3708.0	2.98 ± .65	14.09	0,09	3.42
		4-5	3720.0	2.31 ± .26	14.76	0.00	3.32
		2-3					
		0-1	3745	2.92 ± .18	14.97	0.10	3.40
		1-2	3748.3	3.02 ± .29	14.83	0.11	3.40
	$a^5F_2 - Y^5F^o$	2-2	3763.8	3.12 ± .24	14.70	0.99	4.26
		1-1	3767.2	3.21 ± .35	14.58	1.01	4.28
		3-4	3799.6	2.18 ± .80	14.08	0.95	4.20
	$a^5F - Z^3P^o$	3-2	3812.96	3.91 ± .74	14.73	0.95	4.19
	$a^3F - Y^3D^o$	4-3	3815.9	3.39 ± .30	14.90	1.48	4.71
		3-2	3827.8	3.51 ± .20	14.77	1.55	4.77
	$a^5F - Y^5D^o$	5-4	3820.4	2.88 ± .58	14.72	0.86	4.09
		4-4	3826.0	2.82 ± .40	14.63	0.91	4.14
		1-0	3849.98	3.71 ± 1.30	14.21	1.01	4.21
		1-1	3865.5	3.33 ± .68	14.02	1.01	4.20

1958ApJ...127..680Z

Table 2 (Continued)

Element	Multiplet	J	(A)	β (x 10^8)	log E(0)	E. P. (Volts)	
	$a^5D - Z^5D^o$	4-3	3824.5	3.01 ± .44	14.64	0.00	3.23
		3-2	3856.4	2.91 ± .21	14.75	0.05	3.25
		4-4	3859.9	1.94 ± .23	14.62	0.00	3.20
		2-1	3878.6	2.50 ± .25	14.47	0.09	3.27
		3-3	3886.3	1.75 ± .22	14.57	0.05	3.23
		1-0	3895.5	3.09 ± 15	14.54	0.11	3.28
		0-1	3920.3	2.59 ± .09	14.13	0 12	3.27
		3-4	3922.9	2.60 ± 30	14.20	0.05	3.20
		1-2	3927.9	2.99 ± 34	14.65	0.11	3.25
	$a^3F - Y^3F^o$	3-2	4005.2	3.53 ± 23	14.20	1.55	4.63
		4-4	4045.8	2.58 ± 03	14.54	1.48	4.53
		3-3	4063.6	2.84 ± 06	14.41	1.55	4.59
		2-2	4071.7	2.95 ± .11	14.40	1.60	4.63
		3-4	4143.9	2.92 ± .32	14.12	1.55	4.53
	$a^3F - Z^3G^o$	4-4	4202.0	3.50 ± .30	14.08	1.48	4.42
		4-5	4271.8	2.95 ± .18	14.35	1.48	4.37
		2-3	4325.8	2.73 ± .10	14.43	1.60	4.45
	$Z^7D^o - e^7D$	4-4	4235.9	4.59 ± .55	14.35	2.41	5.33
		5-5	4260.5	3.95 ± 26	14.46	2.39	5.29
	$a^3F - Z^5G^o$	4-5	4383.6	2.62 ± .11	14.52	1.48	4.29
		3-4	4404.8	2.82 ± .12	14.14	1.55	4.35
Fe^+	$b^4P - Z^4D^o$	5/2 - 7/2	4233.2	2.98 ± .18	14.50	2.57	5.49
	$b^4F - Z^4D^o$	3/2 - 1/2	4508.3	4.00 ± 1.30	14.18	-	-
		9/2 - 7/2	4583.8	3.21 ± .13	14.56	2.79	5.49

1958ApJ...127..680Z

Table 2 (Continued)

Element	Multiplet	J	(A)	β (x 10^8)	log E(0)	E.P. (Volts)	
	$b^4F - Z^4F^o$	5/2 - 5/2	4515.3	3.45 ± .51	14.03	2.83	5.57
		9/2 - 7/2	4520.2	3.60 ± 94	14.04	2.79	5.52
	$a^6S - Z^6P^o$	5/2 - 7/2	5169.0	2.96 ± .08	15.04	2.88	5.27
	$a^4G - Z^4F^o$	5/2 - 3/2	5197.6	2.12 ± .36	13.57	3.22	5.59
		7/2 - 5/2	5234.6	2.21 ± .32	13.66	3.21	5.57
Ni	$a^3D - Z^3F^o$	3-4	3414.8	2.35 ± .20	14.10	0.03	3.64
	$a^3D - Z^3D^o$	2-2	3446.3	2.84 ± .17	14.24	0.11	3.69
	$a^3D - Z^3P^o$	2-1	3492.9	2.82 ± .27	14.56	0.11	3.64
Sr^+	$5^2S - 5^2P^o$	1/2 - 3/2	4077.7	1.47 ± .06	14.81	0.00	3.03
		1/2 - 1/2	4215.5	1.85 ± .03	14.82	0.00	2.93
Y^+	$a^3D - Z^3F^o$	3-4	3710.3	3.72 ± .23	14.85	0.18	3.51
		2-3	3774.3	3.43 ± .36	14.67	0.13	3.40
		1-2	3788.7	4.54 ± .46	14.84	0.10	3.36
	$a^3D - Z^1D^o$	2-2	3983.0	4.56 ± .00	14.47	0.15	3.25
Ba^+	$G^2S - G^2P^o$		4554.0	2.91 ± .15	14.88	0.00	2.71

An inspection of Table 2 suggests that the emission gradients depend upon the strength of the lines rather than upon any atomic property, such as ionization or excitation potential. Figure 2 shows β plotted against the integrated emission (E) at 2000 km. The weaker lines have been extrapolated to this height. Note that atoms and ions covering an appreciable range in ionization potential tend to follow the same relation. This behavior suggests that self-absorption (which tends to decrease the emission gradients of strong lines in comparison with weaker lines of the same atom) is the primary factor controlling the magnitude of β. Chromospheric excitation conditions certainly affect the strength of a spectral line but do not seem to fix the emission gradient directly. The effects of self-absorption are revealed clearly by some Fe I lines. Figure 3 shows the variation of β with oscillator strength (King 1942) for eleven lines sharing a^3F as a common lower term. The strong lines (i.e., those with large gf-values) have smaller β than the weak lines.

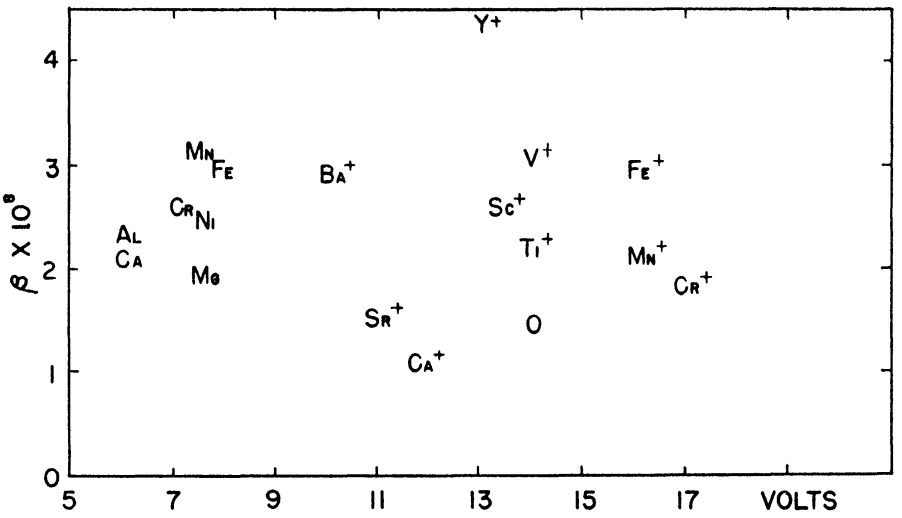

FIG. 1.—The average value of the logarithmic emission gradients of each metallic ion, as a function of ionization potential A strong correlation does not exist.

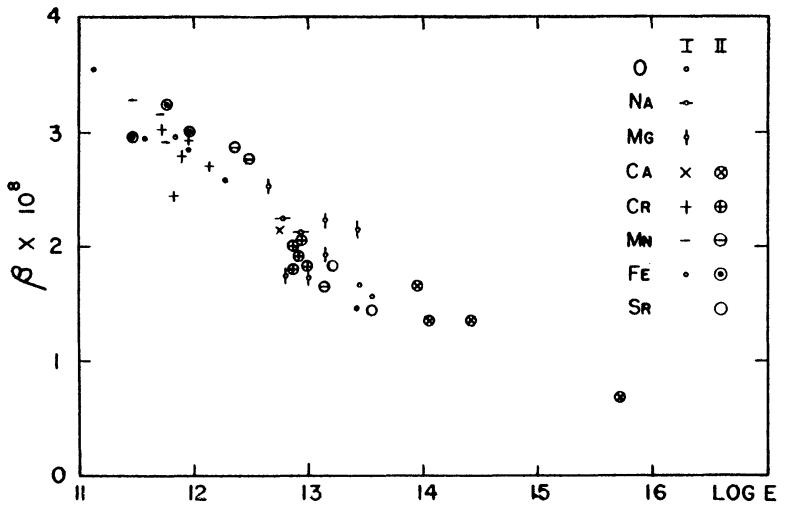

FIG 2 —Emission gradients of neutral (I) and singly ionized (II) metals as a function of integrated emission at 2000 km.

If the metal lines are strongly affected by self-absorption, as the preceding discussion has suggested, the self-absorption must be evaluated before any conclusions may be drawn concerning the populations of emitting and absorbing atoms, i.e., chromospheric excitation conditions. The remainder of this paper is concerned with the evaluation of self-absorption in metal lines and with the resulting information about the mass distribution in the chromosphere.

EVALUATION OF SELF-ABSORPTION

It is reasonable to suppose that at sufficiently great heights (or, equivalently, at sufficiently low intensities) the metal lines are unaffected by self-absorption. Let us assume arbitrarily that the chromosphere is optically thin in any metal line when the integrated emission has dropped to the plate limit (say log $E = 12.00$). At the height (H) corresponding to this intensity, we may equate the emission gradient (β) of a particular line with the gradient (γ) of the number of emitting atoms per cubic centimeter. Figure 4

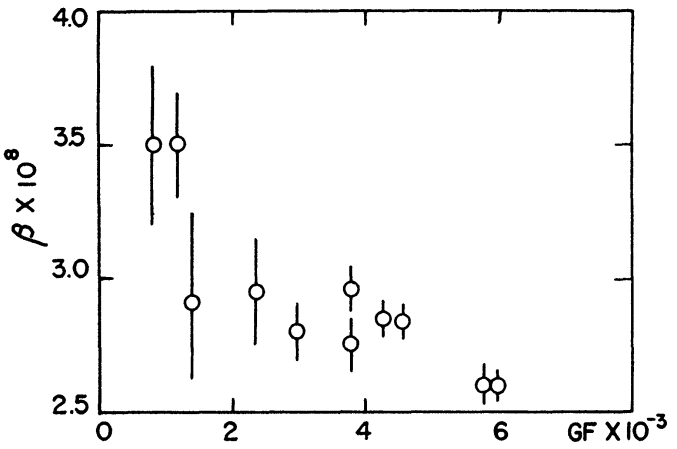

FIG. 3.—Emission gradients versus gf-values for neutral iron lines sharing a^3F as a lower term. Here g is the statistical weight of the lower level and f is the absorption oscillator strength. The presence of self-absorption is indicated.

displays the γ's determined in this manner as a function of H for lines of neutral and singly ionized atoms. To a good first approximation, all metallic atoms, neutral and ionized, exhibit the same variation of γ with height (i.e., the same height variation of scale height).

A simple interpretation of this result identifies the mean γ of the metals, as shown in Figure 4, with the gradient of total density, i.e., the gradient of the number of neutral plus ionized hydrogen atoms per cubic centimeter. The following argument supports this interpretation.

Boltzmann's formula for the concentration of atoms of species r, stage of ionization s, and state t is

$$n_{rst} = \frac{g_{rst} n_{rs}}{u_{rs}} \exp\left(-\frac{\epsilon_{rst}}{kT_{rst}}\right), \tag{1}$$

where g is the statistical weight of state t; u is the partition function; n_{rs} is the total number of r atoms in the sth stage of ionization; ϵ is the excitation potential of state t; and T_{rst} is the excitation temperature relating state t to the ground state. Hence

$$-\gamma_{rst} = \frac{d \ln n_{rst}}{dh} = \frac{d \ln n_{rs}}{dh} - \frac{d \ln u_{rs}}{dh} + \frac{\epsilon_{rst}}{kT_{rst}} \frac{d \ln T_{rst}}{dh}. \tag{2}$$

Now n_{rs} can be written as $n_{rs} = (n_H + n_p)a_r x_{rs}$, where n_H and n_p are, respectively, the hydrogen and proton concentrations; x_{rs} is the fraction of r atoms in the s state of ionization; and a_r is the chemical abundance of r atoms. If a_r is independent of height, equation (2) becomes

$$-\gamma_{rst} = \frac{d \ln (n_H + n_p)}{dh} + \frac{d \ln x_{rs}}{dh} - \frac{d \ln u_{rs}}{dh} + \frac{\epsilon_{rst}}{kT_{rst}} \frac{d \ln T_{rst}}{dh}. \quad (3)$$

Now, according to Figure 4, γ_{rst} has the same height variation for all atoms and ions, i.e. for all r, s, and t. We must conclude that for all atoms and ions the last three terms of equation (3) are either the same or negligible compared with the first term.

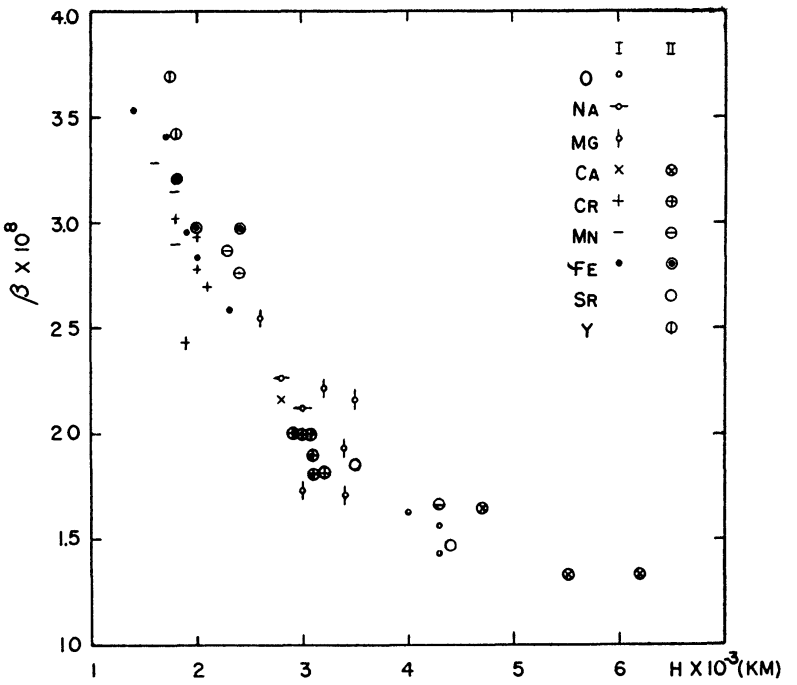

FIG 4.—Emission gradients of neutral (I) and singly ionized (II) metals at the height (H) where the line intensities fall to the plate limit (log E = 12 00).

It seems more reasonable to choose the second alternative, although we have no a priori knowledge of the ionization and excitation of metal atoms in a region which is likely to depart from local thermodynamic equilibrium (LTE). Calculations on the statistical equilibrium of metal atoms, though rather difficult, would be most useful in clarifying this point and in interpreting excitation and ionization temperatures in terms of the electron temperature.

It should be noted here that the assumption of spherical symmetry is implicit in the identification of γ with β at $h = H$. If emitting atoms are confined to a relatively small fraction of the volume, as appears likely from the appearance of the Ca, H, and K lines and Hα above ~5500 km (Athay and Roberts 1955), then γ must change more slowly with height than β, i.e., than is indicated in Figure 4. In the following discussion we shall ignore this possibility at the lower levels of metallic emission.

The analysis of the metal lines for self-absorption may proceed independently of the particular interpretation applied to Figure 4, as follows.

Assume T_{rst} (or, more simply, T_{cx}) to be independent of height for each metal line. Then the gradient of absorbing atoms equals the gradient of emitting atoms:

$$\frac{d \ln n_{rst}}{dh} = \frac{d \ln n_{rsv}}{dh} = -\gamma(h) .$$

Here $\gamma(h)$ is the empirical function of Figure 4, which may be represented by

$$10^8 \gamma(s) = 1.12 + 0.10\, s + 0.005\, s^2 + 0.003\, s^3 + 0.0012\, s^4 . \tag{4}$$

with $h = 7 - s$ measured in 10^3 km. Now if the profile of the absorption coefficient for each metal line is independent of height, we have

$$\frac{d \ln n_{rsv}}{dh} = -\gamma(h) \simeq \frac{d \ln \tau_0}{dh}, \tag{5}$$

where τ_0 is the optical depth in the line center.

TABLE 3

HEIGHT VARIATION OF OPTICAL DEPTHS

h (cm$\times 10^{-8}$)	$G(h)$	$\tau_0(h)$	h (cm$\times 10^{-8}$)	$G(h)$	$\tau_0(h)$	h (cm$\times 10^{-8}$)	$G(h)$	$\tau_0(h)$
0 0	0 00	....	1 5	6 84	16 2	4 0	12 69	0 047
0.5	2 71	1000	2 0	8 41	3 3	5 0	14 23	0 010
1 0	4 97	104	3 0	10 86	0 29	6 0	15 52	0 0027

Thus, from equations (4) and (5),

$$\tau_0(h) = \tau_0(0.5) \exp - \left[\int_{0\,5}^{h} \gamma(t)\, dt\right] \tag{6}$$

is the height variation of the tangential optical depth in any metal line. Table 3 lists the function

$$G(h) = \int_0^h \gamma(t)\, dt$$

and the variation of $\tau_0(h)$ for $\tau_0(0.5) = 10^3$.

We are now in a position to compute theoretical curves of log E versus height. The line profile at the height h is given by

$$I_\lambda(h) = \int_0^{\tau_\lambda(h)} B_\lambda \exp -(t_\lambda)\, dt_\lambda = B_\lambda \left\{1 - \exp\left[-\tau_0(h) \exp -\left(\frac{\Delta\lambda}{\Delta\lambda_D}\right)^2\right]\right\} . \tag{7}$$

The flux is therefore

$$F = 4\pi \int_0^\infty I_\lambda d\lambda = 8\pi \Delta\lambda_D B_\lambda \Phi[\tau_0(h)] . \tag{8}$$

The function $\Phi[\tau_0]$ has been tabulated by Araki (1954). The integrated emission follows from numerical integration of the flux with respect to height:

$$E = \int_h^\infty F(t)\, dt = 8\pi \Delta\lambda_D B_\lambda \int_h^\infty \Phi[\tau_0(t)]\, dt ,$$

where $\tau_0(h)$ is given by equation (6). Figure 5 illustrates the family of curves resulting from different choices of $\tau_0(0.5)$.

These curves, when matched to the observations, yield the parameters $\tau_0(0.5)$ and $B_\lambda(T_{ex})$ for each metal line. Figures 6 and 7 show some typical lines, and Table 4 lists the corresponding values of $\tau_0(0.5)$ and T_{ex}

The fit of the theoretical curves to the observations is satisfactory. Weak lines are free of self-absorption and thus exhibit the steep density gradient of the low chromosphere in their large emission gradients. Self-absorption in a strong line masks the large density gradient at low heights. At greater heights, where the chromosphere is optically thin in the strong line, the density gradient is small. Thus the strong lines show approximately constant emission gradients through the combined effects of self-absorption at low heights and a diminishing density gradient at large heights.

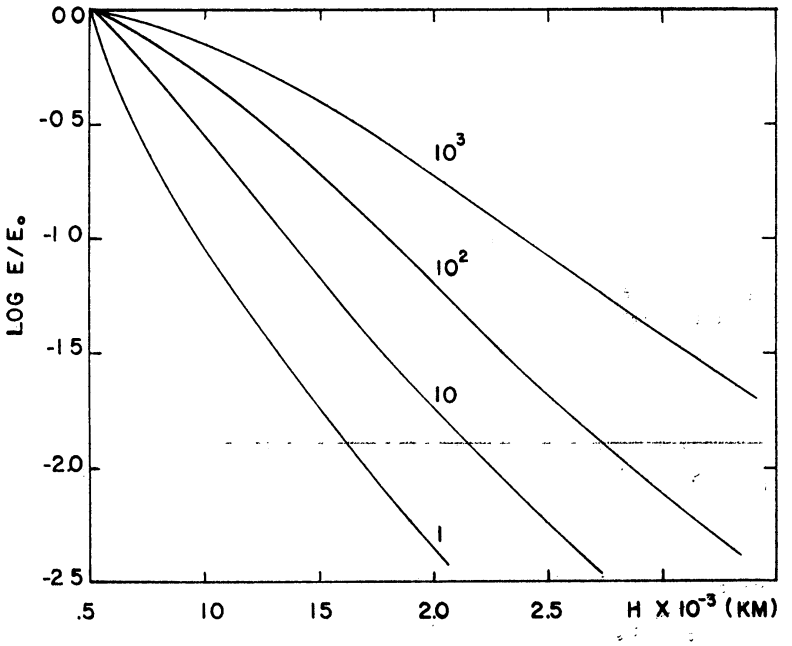

FIG. 5.—Theoretical curves of integrated emission versus height The parameter is the tangential optical depth in the line center at 500 km The curves are normalized to the emission at 500 km.

Table 5 shows that, while the empirical values of $\tau_0(0.5)$ within a multiplet of Ti II are not always proportional to the sum-rule intensities, discrepancies larger than a factor of 2 are rare. An uncertainty of 0.5 in log $\tau_0(0.5)$ corresponds to an uncertainty of 0.3 in log B_λ (see Fig. 5) or 900° for Ti II λ 3510 and 2300° for Ca II λ 8542. The variation of T_{ex} among multiplets of Ti II and of Ca II is readily explained by this source of error.

Thus the preceding method of analysis is too rough to define accurately differences of excitation and ionization among various atomic species. The optical depths in the transition array (d^2s–d^2p) of Ti II lead to an average T_{ex} in the following way. The optical depth for a line in the transition array may be written as

$$\log \tau_0 = C + \log \frac{s}{\Sigma s} + \log S - \frac{5040\epsilon}{T_{ex}},$$

where C is a constant for the array; $s/\Sigma s$ is the relative strength within a multiplet (Russell 1936); S is the relative multiplet strength (Goldberg 1935); and ϵ is the lower

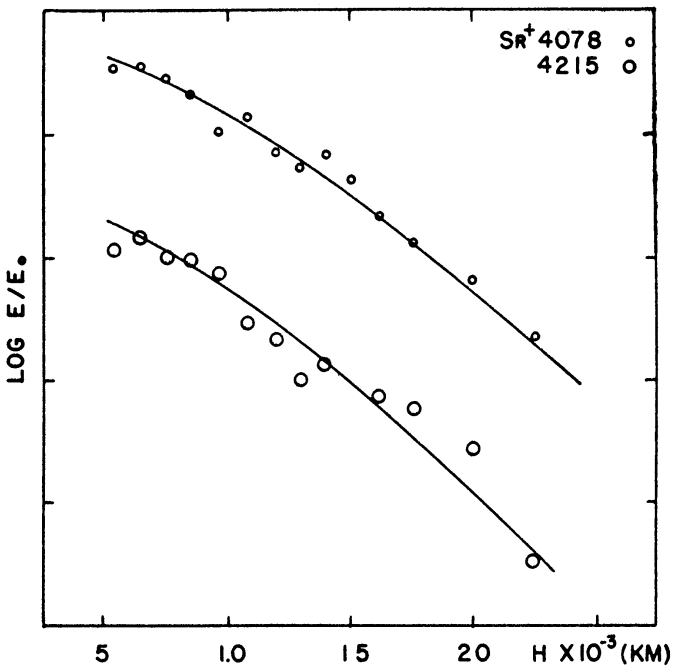

FIG. 6.—Comparison of predicted and observed emission. Each division in the ordinate equals 0 5 in the logarithm. The vertical separation between the two sets of observations is arbitrary.

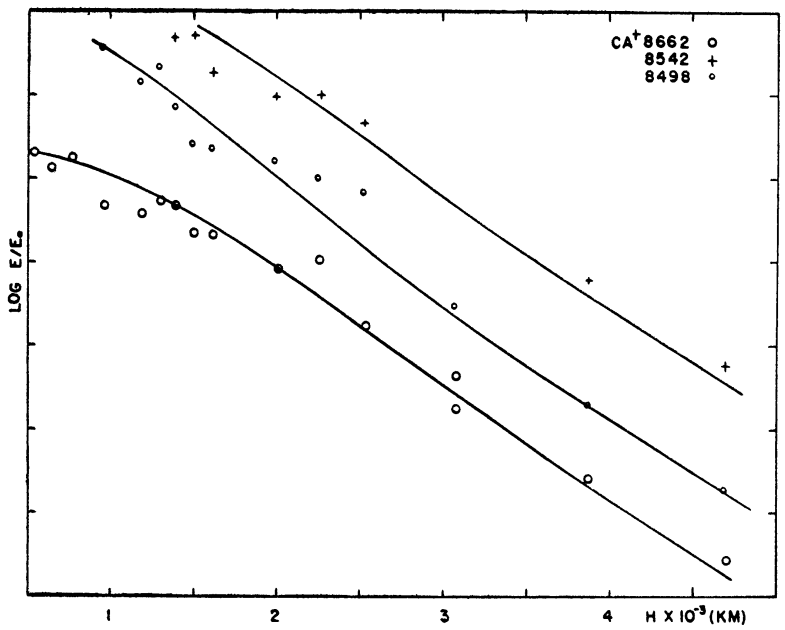

FIG. 7.—Comparison of predicted and observed emission. Each division in the ordinate equals 0 5 in the logarithm. The vertical separation between the three sets of observations is arbitrary.

TABLE 4

EMPIRICAL PARAMETERS

λ	τ	Sum-Rule Intensity	T_{ex} (° K)
Sr II 4078	300	2	5900
4215	150?	1	5700
Ca II 8542	1000	18	8400
8662	1000	10	5900
8498	300	2	6600

TABLE 5

EMPIRICAL PARAMETERS FOR TI II LINES

Multiplet	λ	τ	log $(sS/\Sigma s)$	ϵ (Volts)
	d^2s-d^2p			
$a^4F-z^4G°$	3361	30	+0 97	0 03
	3373	300	+ 84	0 01
	3380	30	− 08	0 05
	3384	300	+ 72	0 00
	3394	100	− 08	0 01
$b^2G-y^2G°$	3504	5	+ 98	1 88
	3510	5	+ 89	1 88
$b^2P-y^2P°$	3456	5	+ 53	2 05
$a^2D-z^2F°$.	4395	30	+ 91	1 08
	4444	20	+ 75	1 08
	4451	3	− 39	1 08
$a^2D-z^2D°$	4294	20	+0 75	1 08
	d^3-d^2p			
$a^2H-z^2G°$	4550	10	2 56	1 58
	4572	20	2 47	1 56
$b^4F-z^4G°$	3444	10	1 78	0 15
	3461	10	1 67	0 13
	3491	30	1 42	0 11
$b^2D-y^2D°$	3742	3	1 77	1 57
$a^2P-z^2S°$	3641	3	1 67	1 23
$a^2P-z^2D°$	4564	10	1 48	1 22
$a^2G-z^2F°$	4469	30	2 27	1 13
	4501	20	2 16	1 11
$a^4P-z^4D°$	4300	5	2 13	1 18

excitation potential. The slope of the log τ_0 versus ϵ plot corresponds to an average T_{ex} of 6100° ± 1100° (see Fig. 8).

Since the intensity at which self-absorption is negligible was fixed arbitrarily at log E = 12.0, the height scale of Figure 4 is arbitrary. Hence, to some extent, the values of $\tau_0(0.5)$ and T_{ex} obtained above are also arbitrary. However, the uncertainty introduced by the choice of log E = 12.0 is not likely to be so serious as the uncertainty inherent in the extrapolation of $\gamma(h)$ to heights below 1500 km. The optical depths and the quantities derived from them in the following sections must therefore be regarded with some caution.

DISCUSSION

Optical depths in the resonance lines of singly ionized metals lead to an estimate of the number of hydrogen atoms/cm³ in the low chromosphere. The number of absorbing

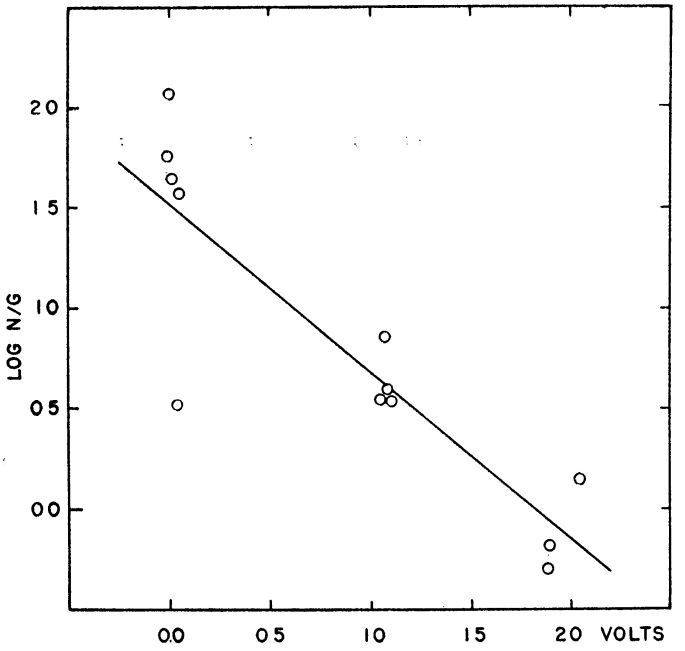

FIG 8.—The Boltzmann distribution of Ti II atoms: concentration of absorbing atoms versus excitation potential. The slope of the line corresponds to T_{ex} = 6100° ± 1100° K.

atoms/cm³ was computed for four such lines from their optical depths. Allen's tabulation of oscillator strengths (1955) and the assumption of thermal broadening at T = 6000° were employed in the calculation. Then hydrogen densities follow from the chemical abundance of each ion (Unsöld 1946; Claas 1951) and the Boltzmann formula, under the assumption that singly ionized atoms predominate. Resonance lines were chosen in order to eliminate any assumption of an excitation temperature linking the lower state of each line with the ground state of the atom. Only the partition functions used in the calculation depend upon the assumption of LTE. Table 6 lists the results of the calculations.

The four estimates in Table 6 show a range of about 1 in log n_H. The determination from λ 4078 probably deserves the highest weight (note the good fit of theory and observation in Fig. 6), but it is probably best from the present analysis simply to admit an uncertainty of about 1 in log n_H, with a value in the range 13–14.

This result may be compared with the determination of n_H from the 1952 eclipse observations of the continuum (Athay *et al.* 1955). In the discussion cited, the emission

at λ 4700, where the H^- continuum dominates, was compared with the emission in the Balmer free-bound continuum to provide what the authors believed to be a quite sensitive determination of the value of T_e, the electron temperature. Actually, this method provides a sensitive measure of n_H rather than T_e, as we see by the following argument. To fix T_e, we must know the departure from the Saha prediction of the occupation number of the ground state. The above-cited analysis assumed no departure from the local thermodynamic equilibrium prediction.

The observations of the Balmer continuum give

$$n_e n_p T_e^{-3/2} = f_1(h) , \tag{9}$$

while the emission at λ 4700 gives

$$n_e + 1.85 \times 10^{13} n_e n_H T_e B(T_e)\, \alpha(T_e) = f_2(h) , \tag{10}$$

where $f_1(h)$ and $f_2(h)$ are empirical functions of height. For any assumed T_e, equation (9) yields n_e, and n_H follows from equation (10). (The ionization of hydrogen is sufficiently complete that $n_e = n_p$.) Table 7 shows the solutions obtained at 500 km, using the

TABLE 6

DETERMINATIONS OF THE HYDROGEN DENSITY AT 500 KM

λ	τ	log n_H	λ	τ	log n_H
Sr II 4077	300	13 7	Ti II 3389	300	13 3
Sc II 3614	3	12 9	Ba II 4554 .	10	12 9

TABLE 7

SOLUTIONS

T_e (° K)	log n_e	log n_H	log b_1	T_e (° K)	log n_e	log n_H	log b_1
5000	11 62	14 24	−1 75	6500	11 71	13 80	+0 98
5500	11 65	14 10	−0 60	7000	11 73	13 74	+1 68
6000	11 67	13 95	+0 31	8000	11 78	13 71	+2 84

empirical values of f_1 and f_2 from the paper cited. The last column contains the non-equilibrium factor, b_1, which represents the ratio of n_H to the value predicted from the Saha equation using the values of T_e and n_e given. Note that the actual value of n_H depends very little on the value of T_e in the range $5000° < T_e < 8000°$, which seems to be the rough range permitted by all the data.

It is clear that the results of Tables 6 and 7 do not differ greatly. Indeed, in view of the uncertainties in empirical data, we must consider the agreement to be quite good. Since the results in Table 6 lie on the low side of those in Table 7, we might have a tendency to believe that the b_1 values probably exceed unity at this 500-km height. This conclusion must be considered tentative, in view of the uncertainties inherent in the analysis. In addition to those mentioned above, we should mention the uncertainty entering through the assumption of a T_{ex} constant with height.

We now turn to another conclusion based upon the optical depths in the metallic lines. We refer to the heights of formation of Fraunhofer lines and the implication of low chromospheric excitation temperatures. Under the assumption of a spherically symmetric chromosphere, the tangential optical depths deduced above may be combined with the empirical height dependence $\tau_0 \sim \exp G(h)$ to give the height H_1 at which the radial optical depth in a line center reaches unity. Table 8 lists these heights of formation

TABLE 8

HEIGHTS OF FORMATION OF FRAUNHOFER LINE CENTERS

Element	λ	H_1 (km)	Rowland Intensity	T_{ex} (° K)
O	7772 0	4×10^2	2	5200
	7774 2	7	2	5300
	7775 4	8	1	5400
Na	5890 0	3	30	3850
	5895 9	2	20	3850
Mg	3829 4	6	10	3850
	3832 3	4	15	3750
	3838 3	6	25	3750
	5167 3		15	3950
	5172 7	2	20	3900
	5183 6	3	30	3800
Al	3944 0	.	15	4050
	3961 5	3	20	4000
Ca	4226 7	3	20	3350
Ca+	3968 5	2×10^3	700	3950
	8498 1	6×10^2	12	4050
	8542 1	9	16	3700
	8662 1	9	15	3800
Ti+	3361 2	2	8	4600
	3372 8	7	5	4500
	3380 3	2	3	4850
	3383 7	4	3	4900
	3394 6	2	3	5000
	3491 1	2	5	5150
	4294 1	1	5	4400
	4395 0	2	3	4550
	4443 8	1	5	4450
	4468 5	2	5	4450
	4501 3	1	5	4700
Cr+	3368 1	8×10^2	5	4700
	3408 8	5	3	5100
	3421 3	5	4	5100
	3422 7	5	4	4700
	3433 3	4	3	5000
Mn+	3442 0	7	6	4650
	3460 3	4	4	4750
	3474 1	3	2	4800
Fe	3859 9	4	20	4200
	3886 3	6	15	4200
Sr+	4077 7	6	8	4000
	4215 5	5	7	4000

of the line core for several lines of interest. The heights of formation depend logarithmically on the empirical optical depths and hence are insensitive to errors in the optical depths. Note that even relatively weak lines of singly ionized metals in the Fraunhofer spectrum (Rowland intensity ~10) have a chromospheric contribution.

The H line of Ca II, λ 3968, was treated separately in this calculation. A set of theoretical curves, similar to those in Figure 5, was determined for the case of an appreciable contribution from radiation damping to the line-absorption coefficient. The optical depth along the line of sight at 500 km is of the order of 10^5 at the center of the H line. This optical depth implies a height of formation of about 2×10^3 km for the line center. Spectroheliograms taken in the center of the Ca II K line would, therefore, pertain to height somewhat greater than 2×10^3 km.

The last column of Table 8 gives the Planck (or excitation) temperature corresponding to the central intensities of the Fraunhofer lines, as measured in the Utrecht atlas Since no correction was made for scattered light, the inferred excitation temperatures are crude upper limits. In many cases these temperatures are lower (sometimes by several thousand degrees) than the corresponding electron temperatures deduced by Athay *et al.* Moreover, as we have seen, Athay's temperatures may be too low. Thus there is clear evidence that the metals depart from thermodynamic equilibrium in the chromosphere. Any attempt to account for the central intensities of metal lines must allow for these departures.

This paper represents a portion of the author's doctoral dissertation (Harvard University, 1956) and has been circulated as a Technical Report of High Altitude Observatory through ONR Contract Nonr 393(01). The research at Harvard University was supported by the Air Force Cambridge Research Center, Geophysics Research Directorate, under Contract AF19(604)-146 with Harvard University.

The author wishes to thank Dr. R. N. Thomas and Dr. R. G. Athay for their interest and encouragement at all stages of this investigation.

REFERENCES

Allen, C. W. 1955, *Astrophysical Quantities* (1st ed ; London: Athlone Press, University of London), p. 74.
Araki, K. 1954, *Pub. Astr. Soc. Japan*, **6**, 109.
Athay, R. G , Billings, D., Evans, J. W , and Roberts, W. O. 1954, *Ap. J.*, **120**, 94.
Athay, R. G., and Menzel, D. H. 1956, *Ap J* , **123**, 285.
Athay, R. G., Menzel, D. H., and Orrall, F. Q. 1956, *Smithsonian Contr. Astrophysics*, **2**, 35.
Athay, R. G., Menzel, D. H., Pecker, J.-C , and Thomas, R. N 1955, *Ap. J. Suppl.*, **1**, 505.
Athay, R. G., and Roberts, W. O. 1955, *Ap. J.*, **121**, 231.
Athay, R. G , and Thomas, R. N. 1955, *Ap. J. Suppl.*, **1**, 491.
Cillié, G. G , and Menzel, D H. 1935, *Harvard Circ.*, No. 410.
Claas, W. J. 1951, *Rech. Obs. Utrecht*, **12**, 13.
Goldberg, L. 1935, *Ap. J.*, **82**, 1.
Hemmendinger, H. 1939, dissertation, Princeton University.
Houtgast, J. 1953, *Convegno Volta, 1952, Roma, Acad Nat. Lincei.*
———. 1957, *Rech. Astr. Obs. Utrecht*, Vol. **13**, No. 3.
King, R. B. 1942, *Ap. J.*, **95**, 78.
Matsushima, S. 1955, *Ap. J. Suppl.*, **1**, 479.
Menzel, D. H. 1931, *Pub. Lick Obs.*, Vol. **17**.
Russell, H. N. 1936, *Ap. J.* **83**, 129.
Unsöld, A. 1946, *Zs. f. Ap.*, **24**, 306.
Vyazanitsyn, V. P. 1956, *IZV. Glavn. Astr. Obs. Pulkova*, **20**, 16.